PREPARATION AND CHARACTERIZATION OF A NUMBER OF OXAZEPANE AND THIAZINANE DERIVATIVES DERIVED FROM SCHIFF BASES AND STUDY OF SOME OF THEIR APPLICATIONS

Hind Majed Abdel Karim*, Salwa Abdel Sattar Jabbar

Department of Chemistry / College of Education for Women / Tikrit University / Iraq.
*e-mail: hind.abdulkarim24@st.tu.edu.iq

Received 21.03.2025 Accepted 06.05.2025

Abstract: This research combines the synthesis of several hexagonal and heptacyclic compounds derived from Schiff bases. The Schiff bases were prepared by incorporating [d][1,3]dioxol-5-carbaldehyde with aniline substituents used as nucleophiles. Several heptacyclic oxazapanes were prepared by incorporating Schiff bases with succinic anhydride, and several hexagonal thiazenanes were prepared by incorporating Schiff bases with 2-mercaptopropanoic acid. Physical and spectroscopic techniques, including infrared, ultravioletvisible, and nuclear magnetic resonance (NMR) spectroscopy, were used to ascertain the compounds' structures. Thin-layer chromatography (TLC) was used to monitor the reaction's progress and ascertain the melting points and purities. Using ultrasonication, chemicals (H9, H13) were transformed into nanocomposites. Scanning electron microscopy (SEM) and X-ray diffraction (XRD) were used for characterization. The effects of several substances on the growth of two distinct bacterial species—one Grampositive (Staphylococcus aureus) and the other Gram-negative (Escherichia coli)—were investigated. Some of the compounds that were synthesized demonstrated substantial inhibitory activity against the bacteria that were being studied, while the antibiotic amoxicillin served as a control. In addition, the prepared compounds (H_9, H_{13}) were evaluated for their ability to inhibit the proliferation of human breast cancer cells (MCF-7) in vitro. The cells were exposed to five different concentrations of the prepared chemicals (31.2, 62.5, 125, 250, and 500 µg/ml), and negative and positive controls. The efficacy of the compounds against breast cancer cells varied. The stability of the compounds against a helium-neon laser was studied when exposed to the laser for 15, 30, 45, and 60 seconds.

Keywords: heterocycle, Schiff bases, nano-compounds, biological activity, MTT, laser.

1. Introduction

Heterocycle research is a perennial area in organic chemistry. Scientists who work in synthetic organic chemistry and the field of natural substances are constantly drawn to it. Because of their wide range of applications, particular chemical reactivity, and natural occurrence, heterocyclic chemistry has been advancing. Compounds with a cyclic structure and two or more distinct types of atoms in the ring are known as heterocyclic compounds [1]. Heterocyclic compounds are found in nature in large quantities and are vital to living things. They are essential to every live cell's metabolism. Nitrogen heterocycles are the most prevalent, particularly those that incorporate oxygen or sulfur [2]. Schiff bases are easily synthesized, structurally varied chemicals often made via condensation reactions between primary amines and a ketone, aliphatic, or aromatic aldehyde [3]. An azomethine (-C=N-) linkage found in Schiff bases can join two or more physiologically active aromatic/heterocyclic scaffolds to create a variety of molecular hybrids with intriguing biological characteristics [4]. In the -C=N-azomethine bond, the nucleophile of nitrogen and the electrophile of carbon provide remarkable binding for joining the electrophilic and nucleophilic functional groups. It has been discovered that if the imine nitrogen atom participates in hydrogen bonding, hydrolytic breakage of the azomethine bond can be avoided in certain Schiff bases, such as the tetromino diphenol macrocyclic Schiff base [5]. In medicinal and pharmaceutical chemistry, Schiff bases are a significant family of commercially used organic compounds with a wide range of biological activities, including anti-inflammatory [6], analgesic [7], antimicrobial [8], antioxidant [9], anticonvulsant [10], antitubercular [11], and anticancer [12], among others. Schiff base derivatives, specifically imine derivatives, are substances created when primary amines and aldehydes condense. They have a wide

range of biological, medicinal, clinical, pharmacological, and analytical uses, and because of their adaptability and simplicity of preparation, they are frequently used as ligand precursors [13]. The nitrogen atom in azomethine is in charge of forming a hydrogen connection with the active centers of cell components and influencing regular cell functions. Producing organic molecules, dyes, pigments, polymers, stabilizers, and corrosion inhibitors all require azomethine compounds as catalysts and intermediates in addition to their biological activity [14].

2. Experimental part

- **2.1. Materials:** Fluka, Aldrich, and BDH supplied all of the compounds utilized in this investigation, and none of them required additional purification.
- **2.2. Devices used:** The Electrothermal Melting Apparatus 9300 measured the melting points. FT-IR 8400S Shimadzu spectrophotometer by KBr disc, 400–4000 cm⁻¹ scale. Bruker equipment operating at 400 MHz produced ¹H-NMR and ¹³C-NMR spectra. Shimadzu UV-1800 spectrophotometer, Tikrit University, having quartz cells ranging from 200 to 800 nanometers. Using Fluka silica gel plates that were 0.2 mm thick and activated with fluorescent silica gel G, Thin Layer Chromatography (TLC) was carried out. UV light was used to see the results. The Raypa steam sterilizer (Spain) autoclave at the University of Tikrit's Advanced Microbiology Research Laboratory was utilized to sterilize the microbiological medium used in the study. In the same lab, Petri dishes utilized for the microbiological investigation were incubated using a Heraeus D-63450 incubator (Germany). A MIRA3-TE SCAN microscope from Belsorp, Czech Republic, was used to perform scanning electron microscopy (SEM). A Shimadze-XRD-6000 instrument was used for an X-ray diffraction (XRD) study at Kashan University in Iran. A 2010 Tikrit University helium-neon laser with a 1-milliwatt power output and an 808-nanometer wavelength was used in visible laser tests.
- **2.3.** Preparation of Schiff base derivatives (H₁-H₅). 0.003 mol of any amino derivative was taken and dissolved in 20 ml of absolute ethanol. Then, 0.003 mol (0.7 g) of 6-bromobenzoate [d][1,3]dioxol-5-carbaldehyde was dissolved in 15 ml of absolute ethanol. This solution was mixed with 3 drops of glacial acetic acid, followed by heating, and was added to the above mixture. The reflux condition of this reaction took 10-14 hours and TLC was used as a monitor for the completion of the response. After the completion of the response, the entire mixture was allowed to cool gradually [15]. It was filtered to collect the precipitate, dried to constant weight, and recrystallized using absolute ethanol (Table 1).
- **2.4. Preparation of 1,3-Oxazapane-7,4-dione derivatives (H₆-H₁₀).** Table 1 shows that when 0.004 mol of the synthesized Schiff bases (H1-H5) were dissolved in 10 mL of dry benzene with 0.4 g, 0.004 mol of succinic anhydride, the mixture was filtered to produce a precipitate, which was then recrystallized using the solvent 1,4-dioxane. After that, the mixture was left to cool for 12 to 15 hours at room temperature [16].
- **2.5. Preparation of 1,3-thiazinan-4-one derivatives (H₁₁-H₁₅).** After mixing 0.004 mol of the prepared Schiff bases (H₁-H₅) with 0.424 g (0.004 mol) of 3-mercaptopropionic acid dissolved in 20 mL of THF, the mixture was stirred for 13–15 h [17]. The completeness of the reaction was verified using TLC, and the product was allowed to cool and neutralize with 10% sodium bicarbonate before being filtered, cleaned with cold water, and recrystallized with THF (Table 1).

Table 1. The physical properties of the prepared compounds (H₁-H₁₅)

Comp.	Ar	Molecular Formula/	Color	M.P	R.T	R_f	Yield
No.		M.Wt g/mol		(⁰ C)	hour		(%)
$\mathbf{H_1}$	$\begin{pmatrix} z \\ z \end{pmatrix}$	C ₁₇ H ₁₁ BrN ₄ O ₂ 383.21	Light	124-126	6	0.62	79
	N.		Purple				
H ₂	ZZ	C ₁₂ H ₈ BrN ₃ O ₂ 306.12	White	131-133	7	0.67	83
Н3	Z Z Z Z	C ₁₃ H ₉ BrClN ₃ O ₂ 354.59	Light yellow	120-122	7	0.63	82

H ₄	N Br	C ₁₂ H ₇ Br ₂ N ₃ O ₂ 385.02	Brown	146-148	7	0.70	77
Н5		C ₁₃ H ₉ BrClN ₃ O ₂ S 386.65	Light green	115-117	6	0.65	81
H ₆		C ₂₁ H ₁₅ BrN ₄ O ₅ 483.28	Orange	245-247	14	0.82	59
H ₇	ZZ	C ₁₆ H ₁₂ BrN ₃ O ₅ 406.19	Light pink	272-274	12	0.87	63
H ₈	r z z z	C ₁₇ H ₁₃ BrClN ₃ O ₅ 454.66	Dark yellow	247-249	14	0.83	62
Н9	N Br	C ₁₆ H ₁₁ Br ₂ N ₃ O ₅ 485.09	Light green	278-280	14	0.90	67
H_{10}		C ₁₇ H ₁₃ BrClN ₃ O ₅ S 486.72	Light Yellow	253-255	15	0.85	61
H ₁₁		C ₂₀ H ₁₅ BrN ₄ O ₃ S 471.33	Light Brown	177-179	13	0.83	61
H ₁₂	ZZZ	C ₁₅ H ₁₂ BrN ₃ O ₃ S 394.24	White	217-219	13	0.76	63
H ₁₃	Z CH ₃	C ₁₆ H ₁₃ BrClN ₃ O ₃ S 442.71	Light Yellow	274-276	15	0.75	67
H ₁₄	N Br	C ₁₅ H ₁₁ Br ₂ N ₃ O ₃ S 473.14	Light Green	232-235	13	0.89	61
H ₁₅	CI N S	C ₁₆ H ₁₃ BrClN ₃ O ₃ S ₂ 474.77	Yellow	198-200	14	0.79	58

- **2.6. Preparation of Nano-Compounds of (H₉, H₁₃).** The mixture is placed on a sonicator for six hours after adding 10 milliliters of 100% ethanol to 0.1 grams of the organic component (H₉, H₁₃). After drying the solution to produce a precipitate, the organic nano compound (H₉, H₁₃) is manually milled into a fine powder [18].
- 2.7. Measuring the laser effectiveness of some prepared compounds. A visible helium-neon laser assessed the efficacy of a few produced compounds (H₁, H₅, H₆, H₈, H₁₂, H₁₃). Physical characteristics and alterations in the produced compounds were noted when the compounds were exposed to radiation for varied lengths of time (15, 30, 45, and 60 seconds) [19].
- **2.8. Biological activity study.** Gram-positive and Gram-negative bacteria and Staphylococcus aureus one of the two dangerous bacterial species examined in this study was Escherichia coli. These bacteria play a crucial role in the medical field due to their resistance to antibiotics. They were sourced from the laboratories of the Department of Life Sciences at the College of Education for Pure Sciences. To assess the biological activity of antibiotics and other medical substances, Molter Hinton agar, a specialized culture medium, was used [20]. It quantifies and ascertains the minimal inhibitory concentration (MIC). DMSO solvent was used to create chemical solutions of (H₁, H₄, H₅, H₇, H₈, H₁₀, H₁₄, H₁₅) at concentrations of 0.1, 0.01, and 0.001 mg/ml. As the inhibition diameter increases, the biological activity of the prepared compounds also increases. Therefore, the results were analyzed the following day to assess the sensitivity of the derivatives used. This sensitivity is determined by the apparent inhibition diameter around the wells, which is compared to the inhibition diameter of the antibiotics [21].
- **2.9. MTT Cytotoxicity Assay.** Three replicates of the cytotoxicity tests were performed, and the IC50 values were calculated. The solute solution used was 3-(4,5-dimethylthiazol-2-yl)-2,5-diphenyltetrazolium bromide (MW = 414) [22]. Following the manufacturer's protocol, breast cancer cells were prepared as previously described. The cell suspension was then added to a 96-well plate at a concentration ranging from 1×10^4 to 1×10^6 cells/ml, with each well receiving 200 µl of complete culture medium. Sterile parafilm was used to seal the plates, which were then gently shaken and incubated. Following incubation, 200 µl of the control sample and the prepared concentrations of the compounds under study (31.2, 62.5, 125, 250, and 500 µg/ml) were added to each of the three wells. The mixture was then incubated in a 5% CO₂ incubator for 24 hours at 37°C. After exposure to the

tested compounds, $10~\mu l$ of MTT solution were added to each well. The plate was then incubated for an additional four hours at $37^{\circ}C$ in a 5% CO₂ incubator. Following this, $100~\mu l$ of DMSO was added to each well and left for five minutes. The absorbance was then measured at 570~nm using an ELISA reader [23]. The IC50 was determined by statistically analyzing the optical density measurements.

2. Results and discussion

The compounds were synthesized as in Scheme 1.

Scheme 1. Route of prepared compounds (H₁-H₁₅)

3.1. Characterization of Schiff base derivatives (H₁-H₅). When studying the UV-visible spectrum of the [H₁-H₅] compounds in absolute ethanol as a solvent and at a molar concentration between [10^{-5} and 10^{-4}] of the prepared compounds, short wavelengths (λ_{min}) appeared at 217-251 nm, which are attributed to the ($\pi \rightarrow \pi^*$) transition, while long wavelengths (λ_{max}) appeared at 315-383 nm, which are attributed to the ($n \rightarrow \pi^*$) transition.

The bands linked to the amine group (NH₂) were not present in the FTIR spectrum of the produced Schiff bases [H₁-H₅]. Instead, an absorption band in the range 3087-3034 cm⁻¹ was seen, which is explained by the aromatic (C-H) bond stretching. Additionally, the aliphatic (C-H) bond's symmetric and asymmetric bands were detected at 2862-2831 cm⁻¹ and 2971-2931 cm⁻¹, respectively. The (C=N) group is responsible for a medium-sized band in the frequency range of 1620-1610 cm⁻¹ among the spectral bands. Two bigger bands at 1481-1456 cm⁻¹ and 1682-1565 cm⁻¹ are visible in this band, which are ascribed to the aromatic (C=C) bond stretching. Additionally, the symmetric and asymmetric stretching of the (C-O-C) bond is responsible for the appearance of a medium and firm absorption band at 1305-1274 cm⁻¹ and 1381-1336 cm⁻¹. The (C-N) type bond was vigorously stretched at 1229-1261 cm⁻¹ in the spectrum [24], as seen in Fig.s 1 and 2 and Table 2.

Table 2. Uv-Viv and FT-IR absorption results for Schiff base derivatives (H₁-H₅)

	λ		IR (KBr) cm ⁻¹								
	max ₁	Ar	ν (C-	ν (C-	ν(C=	ν	ν C-O-	ν(C-	Others		
Co	λ		H)	H)	N)	(C=C)	C	N)			
mp.	max ₂		Arom.	Aliph.		Arom.	sym.				
No.	EtO			_			asy.				
	H										
	nm										
H_1	228		3086	2862	1610	1456	1290	1242	-		
	380	N 🌙		2970		1577	1336				

H_2	229	Z N	3060	2852	1620	1461	1274	1257	
	315	- N		2931		1582	1381		
H ₃	227	N CH₃	3087	2858	1615	1472	1286	1261	(723) υ (C-
	380	CI		2971		1565	1376		Cl)
H_4	217	N Br	3056	2831	1620	1481	1305	1240	(692) υ (C-
	332	N		2939		1577	1340		Br)
H ₅	251	CI N	3034	2849	1618	1473	1287	1229	(731) υ (C-
	383	S, N		2935		1573	1356		Cl)

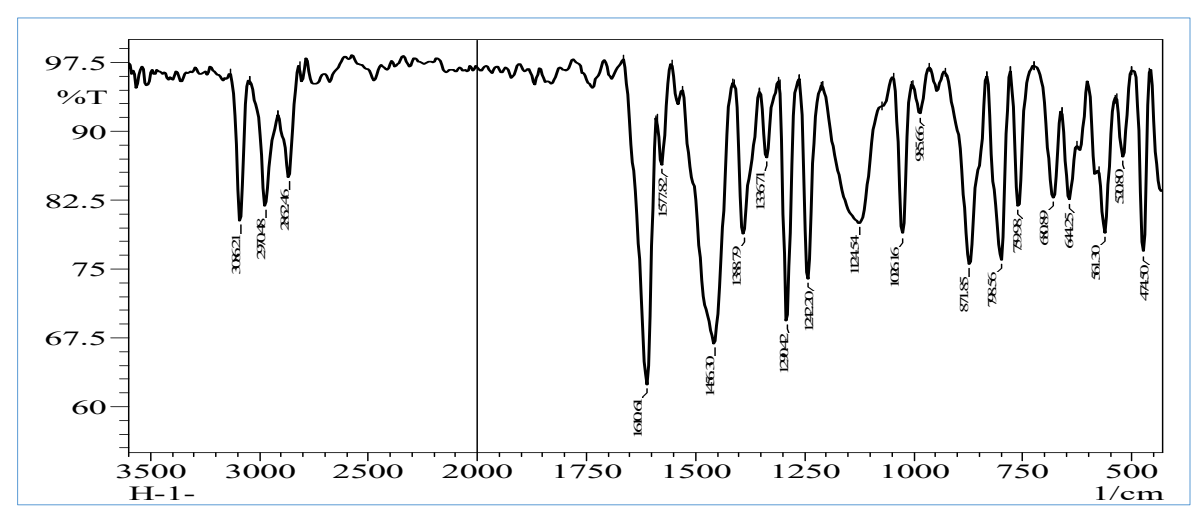


Fig. 1. FT-IR spectrum of the (H₁) compound

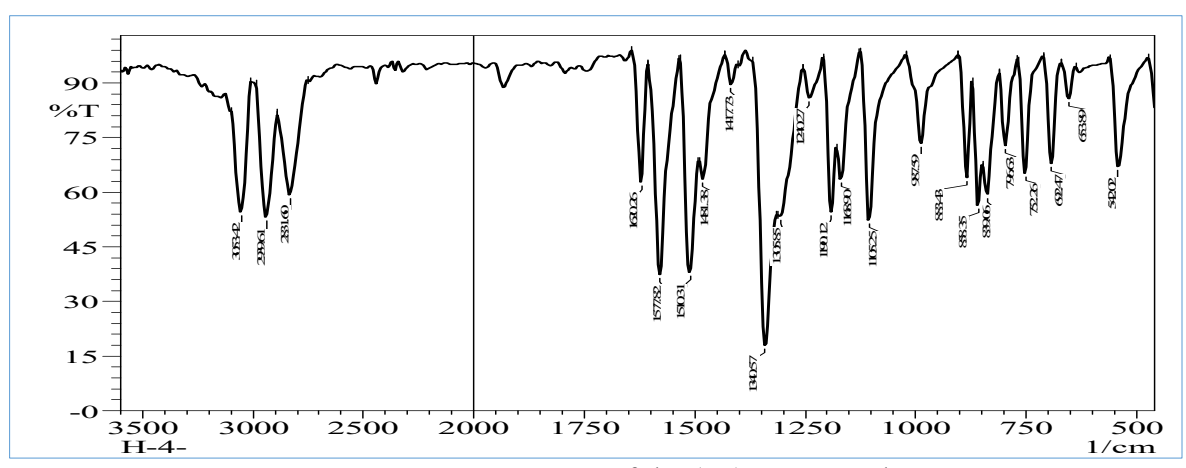


Fig. 2. FT-IR spectrum of the (H₄) compound

When the 1 H-NMR spectrum of compound [H₃] in solvent (DMSO-d6) was analyzed, one signal was observed at position (δ H=8.79 ppm) attributed to the protonation of the amino group (N=C-H), and two signals were observed at position (H=7.79, 7.23 ppm) attributed to the C-H-Ar group. The spectrum showed one signal at position (δ H=7.50 ppm) associated with the C-H-Ar proton in the pyrimidine ring, one signal at position (δ H=4.36 ppm) associated with the CH₂ proton, and one signal at position (δ H=2.09 ppm) associated with the CH₃ proton, as illustrated in Figure 3. When analyzing the 13 C-NMR spectrum of [H₃], a single signal was observed at the δ ¹³C=(160.01) ppm shift, which was attributed to carbon (N=C-H). The observed spectrum indicates that the signals

ppm shift, which was attributed to carbon (N=C-H). The observed spectrum indicates that the signals δ^{13} C=(118.02 - 146.62) ppm are from the aromatic carbon ring (C-H-Ar). A single signal at the δ^{13} C=(112.63) ppm shift was attributed to carbon (CH₂), while a single signal at the δ^{13} C=(49.39) ppm shift was attributed to carbon in the (CH₃) group (Fig. 4).

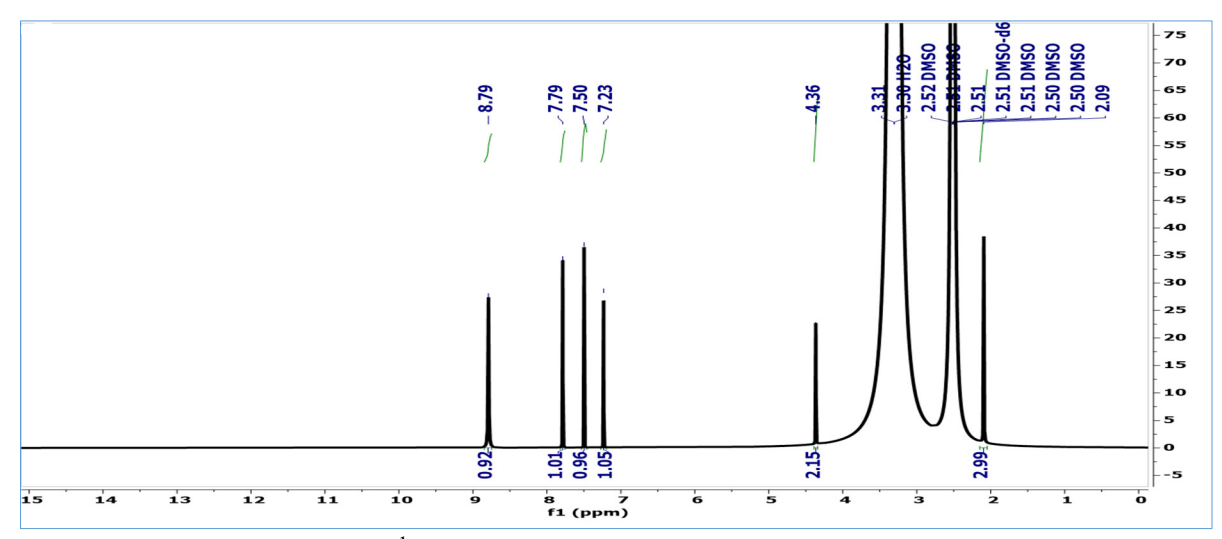


Fig. 3. ¹H-NMR spectrum of the (H₃) compound

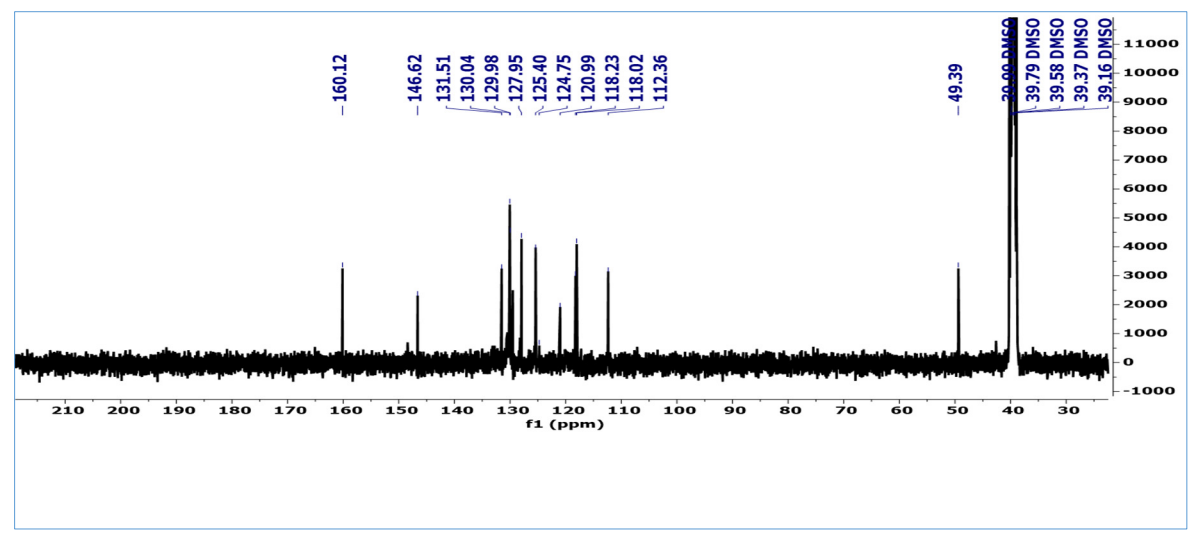


Fig. 4. ¹³C-NMR spectrum of the (H₃) compound

3.2. Characterization of 1,3-Oxazepane-7,4-dione derivatives (H₆-H₁₀). When studying the UV-visible spectrum of the compounds [H₆-H₁₀] in ethanol (95%) as a solvent and at a concentration between [10^{-5} - 10^{-4}] molar for the prepared compounds, short wavelengths (λ_{min}) appeared at 217-251 nm, which are due to the ($\pi \rightarrow \pi^*$) transition, with long wavelengths (λ_{max}) in the range 352-375 nm, which are due to the ($n \rightarrow \pi^*$) type electronic transition.

Due to the presence of the (C=N) group in the prepared Schiff base compounds, the middle band 1620-1610 cm-1 [H₁-H₅] was lost during the infrared spectroscopy of the compounds prepared in this manner [H₆-H₁₀]. The stretching of the carbonyl bond (C=O) of lactone and lactam is responsible for the appearance of two prominent bands with frequencies of 1724–1718 cm⁻¹ and 1690–1672 cm⁻¹, respectively. The aromatic (C-H) bond stretching caused the remaining bands to nearly retain their natural range along the chain derivatives, as seen in the absorption spectrum 3044-3028 cm⁻¹. The stretching of the (C-H) bond is responsible for the appearance of two symmetric and asymmetric bands in the ranges of 2866-2847 cm⁻¹ and 2961-2924 cm⁻¹. Additionally, two aliphatic bands were detected, respectively. The aromatic (C=C) bond's vibrations caused two stretching bands to appear in the ranges of 1502-1456 cm⁻¹ and 1582-1562 cm⁻¹, respectively. Other, more intense bands appeared in the ranges of 1228-1186 cm⁻¹, which are caused by the stretching of the (C-N) bond, and an intermediate band appeared in the ranges of 1255-1307 cm⁻¹ and 1319-1378 cm⁻¹. This is explained by the (C-O-C) bond's symmetric and asymmetric stretching [25], as seen in Fig.s 5 and 6 and Table 3.

Table 3. Uv-Viv and FT-IR absorption results for 1,3-Oxazepane-7,4-dione derivatives (H₆-H₁₀)

			IR (KBr) cm ⁻¹								
	λ	Ar	ν (C-	ν (C-	ν	ν	ν	ν(C-N)	Others		
Com	max ₁		H)	H)	(C=O)	(C=C)	C-O-	ν			
p.	λ		Arom.	Aliph	lactone	Arom.	\mathbf{C}	(C=C)			
No.	max ₂				ν		sym.	Oliph.			
	EtO				(C=O)		asy.	•			
	H				lactam						
	nm										
H_6	251	N	3034	2849	1718	1473	1281	1213			
	353	N		2955	1684	1582	1352				
H_7	217	N	3030	2860	1720	1494	1255	1186			
	352			2943	1685	1581	1319				
H_8	219	YNY ^{CH₃}	3036	2847	1724	1456	1307	1228	υ (C-(746)		
	372	CI		2933	1672	1562	1336		Cl)		
H9	226	N Br	3028	2863	1721	1502	1306	1212	υ (C-(643)		
	365	- N		2924	1687	1580	1378		Br)		
H_{10}	229	ÇI N	3044	2856	1723	1492	1286	1217	υ (C-(734)		
	375	`s^n*		2961	1690	1574	1358		Cl)		

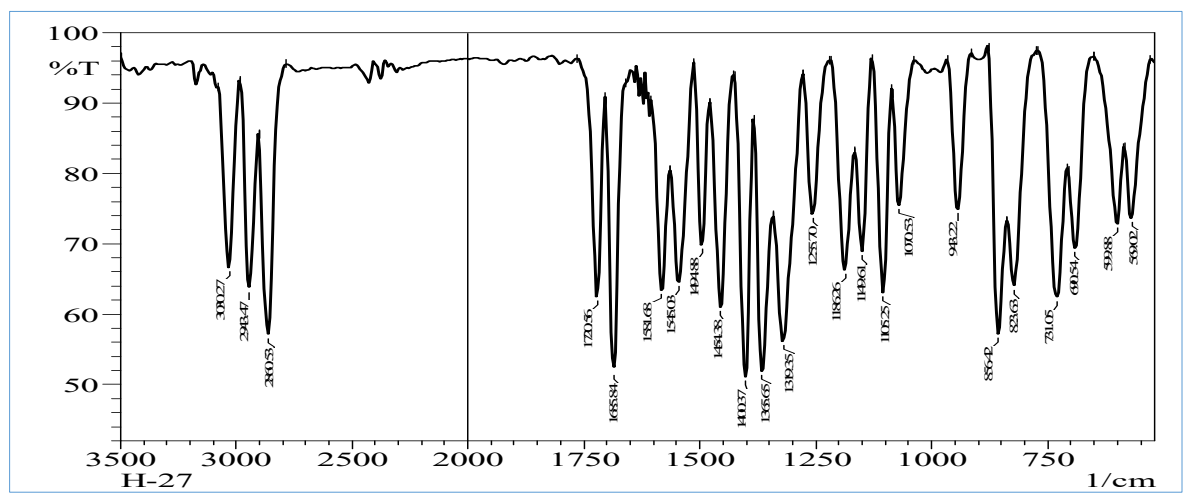


Fig. 5. FT-IR spectrum of the (H₇) compound

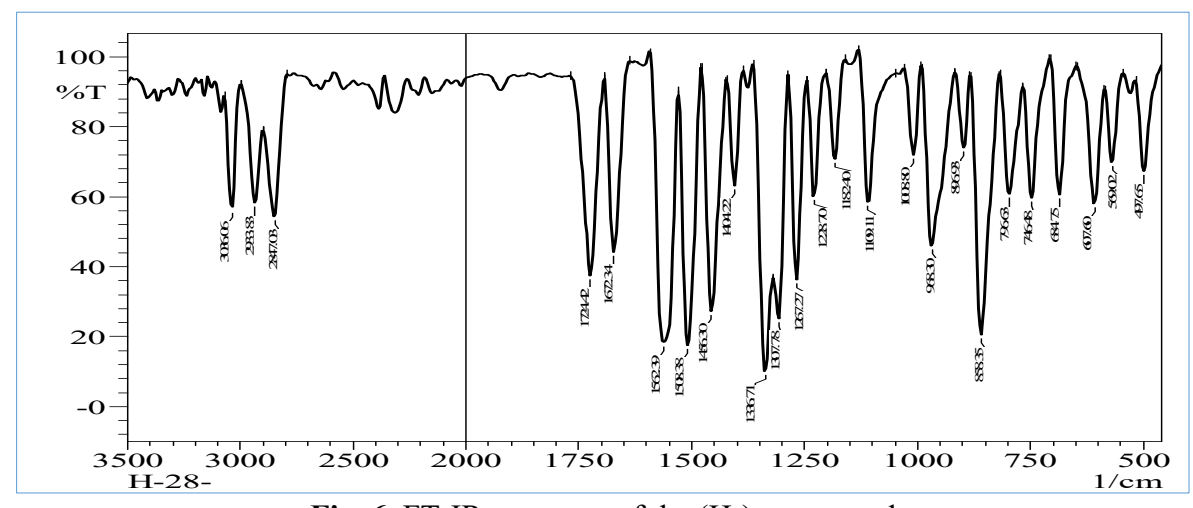


Fig. 6. FT-IR spectrum of the (H₈) compound

While studying the ¹H-NMR spectrum of the compound [H₉], one signal was removed at the position (δH=8.79 ppm) associated with the (N=C-H) group in the prepared Schiff bases [H₁-H₅], and one signal was added at the position (δH=8.24 ppm) associated with the protons of the (CH=N-

pyrimidine) group. Among the spectrum peaks, there were two single signals at (δ H=7.88, 7.36 ppm) attributed to the (C-H-Ar) group, as well as the appearance of a single signal at (δ H=7.07 ppm) attributed to the protons of the C-H group in the seven-membered ring, in addition to the appearance of a single signal at (δ H=6.00 ppm) attributed to the protons of the (CH₂) group, and the appearance of two triple signals at the positions (δ H=1.67-1.63 ppm) and (δ H=1.16-1.12 ppm) attributed to the protons of the (CH₂-CH₂) group in the formed seven-membered ring (Fig. 7).

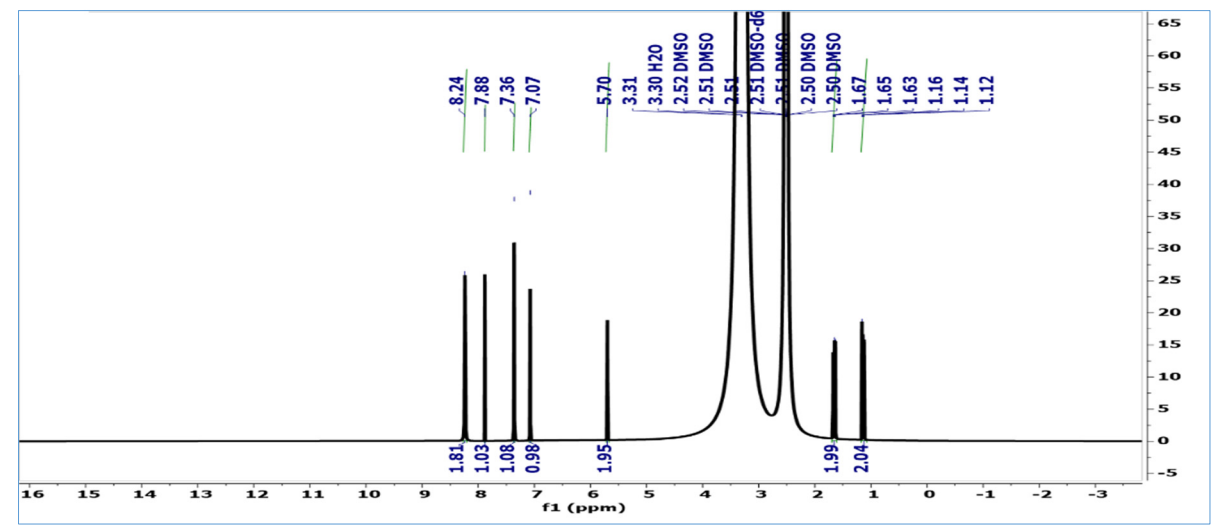


Fig. 7. ¹H-NMR spectrum of the (H₉) compound

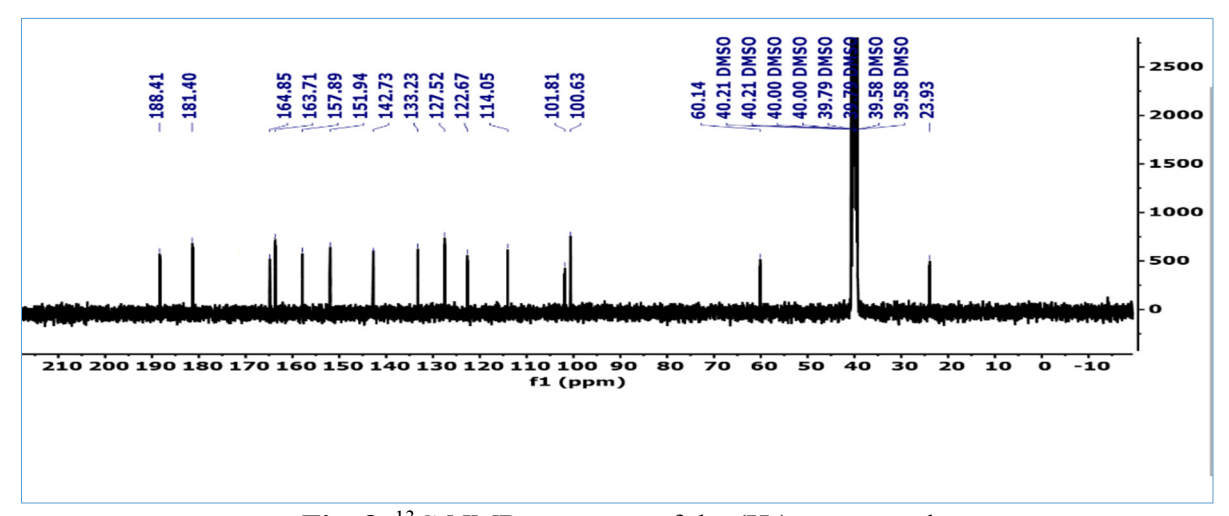


Fig. 8. ¹³C-NMR spectrum of the (H₉) compound

The carbon atom in the (C=O) group of the formed seven-membered ring was identified as the source of two signals at δ^{13} C=(188.41, 181.40) ppm in the 13 C-NMR spectrum of [H₉]. In addition, the carbon atom in the aromatic ring (C-H-Ar) was identified as the source of signals in the range δ^{13} C=(164.85-114.05) ppm, along with a signal at δ^{13} C=(101.81) ppm to carbon (CH₂) and a signal at δ^{13} C=(100.63) ppm identified as the carbon atom (C-H) in the formed oxazepane ring, and the carbon atom (CH₂-CH₂) in the ring was identified as the source of the two signals at δ^{13} C=(60.14, 23.93) ppm, and oxazepanes were produced (Fig. 8).

3.3. Characterization of 1,3-thiazinan-4-one derivatives (H₁₁-H₁₅). While studying the UV-vis spectrum of [H₁₁-H₁₅] compounds in absolute ethanol as a solvent at a concentration of 10^{-5} - 10^{-4} , short wavelengths (λ_{min}) appeared at (251-231) nm, which are attributed to the ($\pi \rightarrow \pi^*$) transition, while long wavelengths (λ_{max}) appeared at 380-321 nm, which are attributed to the ($n \rightarrow \pi^*$) transition.

The band linked to the azomethine group (C=N) that was present in the range of 1620-1610 cm⁻¹ in the prepared Schiff base compounds [H₁-H₅] was found to have disappeared during the infrared spectroscopy of the compounds made in this manner [H₁₁-H₁₅]. Instead, a new band linked to the

(C=O) group in the thiazinane ring appeared in the range of 1578-1666 cm⁻¹. Two absorption bands at 2875-2825 cm⁻¹ and 2963-2932 cm⁻¹ were caused by stretching of the aliphatic (CH₂) bond, and two new bands in the ranges of 1490-1468 cm⁻¹ and 1571-1548 cm⁻¹ were linked to the aromatic (C=C) bond. Additionally, a new band was detected in the range 3080-3049 cm⁻¹, which was linked to the aromatic (C-H) bond. In addition to the appearance of medium and strong absorption bands in the ranges 1303-1244 cm⁻¹ and 1364-1327 cm⁻¹, which resulted from the symmetric and asymmetric stretching of the (C-O-C) bond, the FTIR spectrum also revealed additional bands in the range 1211-1178 cm⁻¹, which were attributed to the stretching of the (C-N) bond [26], as shown in Fig. s 9 and 10 and Table 4.

Table 4. Uv-Viv and FT-IR absorption results for 1,3-thiazinan-4-one derivatives (H₁₁-H₁₅)

				•		IR (KBr)			(1111 1113)
Com p. No.	λ max ₁ λ max ₂ EtOH Nm	Ar	v (C- H) v Arom.	v (C- H) vAliph	v C=O)	v (C=C) Arom.	vC-O- C sym. asy.	ν(C- N) ν (C- S)	Others
H_{11}	248	Z Z	3049	2831	1678	1468	1244	1203	
	373	N=/		2963		1571	1364	862	
H_{12}	231	N N	3080	2875	1677	1490	1290	1178	
	380	- 'N'		2947		1548	1342	825	
H_{13}	237	N CH₃	3058	2853	1666	1485	1257	1196	υ (C-(735)
	375	Çı		2932		1554	1327	827	Cl)
H ₁₄	251	N Br	3071	2862	1669	1468	1248	1211	υ (C-(648)
	372	/`N		2934		1564	1353	846	Br)
H ₁₅	233	CI N	3064	2825	1668	1490	1303	1193	υ (C-(740)
	321	's N		2945		1564	1355	877	Cl)

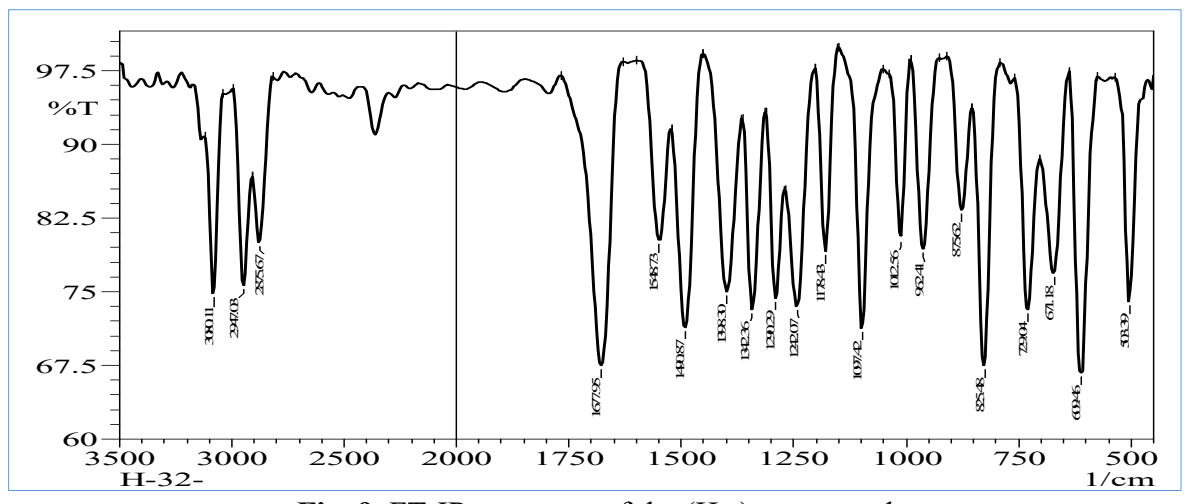


Fig. 9. FT-IR spectrum of the (H₁₂) compound

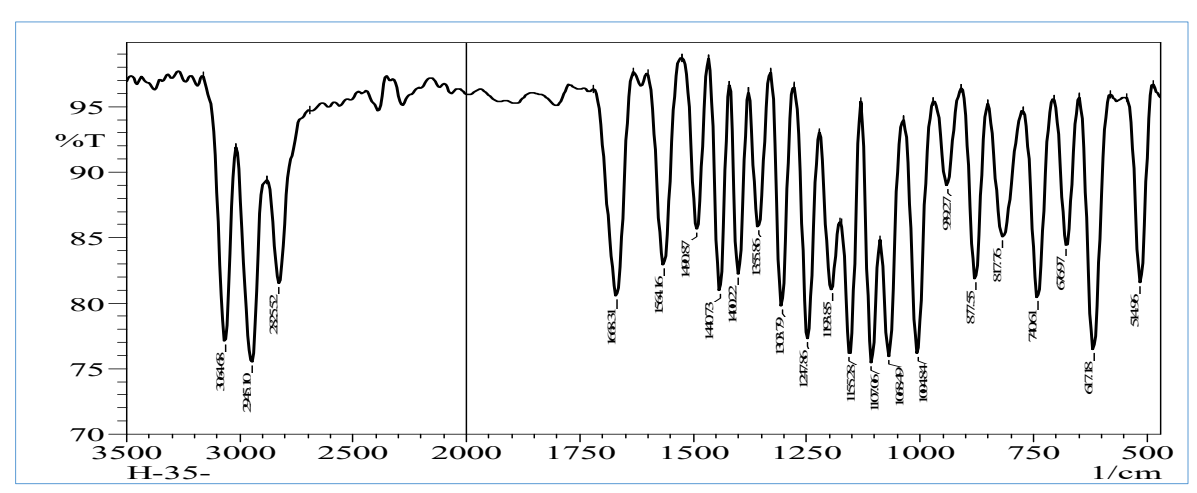


Fig. 10. FT-IR spectrum of the (H₁₅) compound

When the $^1\text{H-NMR}$ spectrum of [H₁₅] was analyzed in DMSO-d⁶, a signal previously present at position ($\delta\text{H=8.79}$ ppm) was observed. This signal was attributed to (N=C-H). A single signal was observed at ($\delta\text{H=7.96}$ ppm) for the protons of the (C-H-pyrimidine) group. The spectrum showed two single signals at ($\delta\text{H=7.65}$, 7.07 ppm) associated with (C-H-Ar), in addition to a single signal at ($\delta\text{H=6.56}$ ppm) associated with (CH₂). One signal was observed at ($\delta\text{H=6.17}$ ppm) and attributed to the protons of the (C-H) group in the formed hexagonal ring, and one signal was observed at ($\delta\text{H=2.34}$ ppm) and attributed to the protons of the (CH₃) group. Two triplet signals at positions ($\delta\text{H=2.14-2.07}$ ppm) and ($\delta\text{H=1.24-1.18}$ ppm) were attributed to the protons of the formed hexagonal (CH₂-CH₂) (Fig. 11).

During the study of the 13 C-NMR spectrum of the compound [H₁₅], signals were observed in the range δ^{13} C = 172.85-102.62 ppm, which are attributed to the carbon atoms in the aromatic rings (C-H-Ar); a signal at δ^{13} C = 15.60 ppm, which is attributed to the carbon atom in the (C=O) group; and a signal at δ^{13} C = 100.34 ppm, which is attributed to the carbon atoms in the (CH₂) group. In addition, a signal was observed at δ^{13} C = 61.68 ppm, which is attributed to the carbon atom in the (C-H) group, and two signals were observed at the position δ^{13} C = 30.84 and 19.01 ppm, which are attributed to the two carbon atoms in the (CH₂) group. In addition, a signal was observed at δ^{13} C = 15.60 ppm, which is attributed to the carbon atom in the (CH₃) group (Fig. 12).

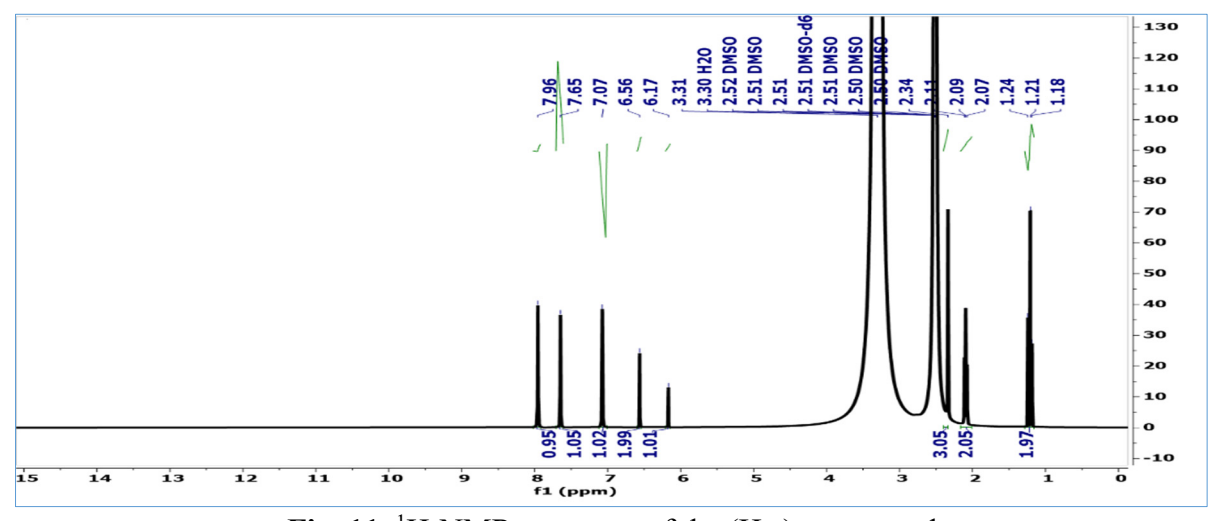


Fig. 11. ¹H-NMR spectrum of the (H₁₅) compound

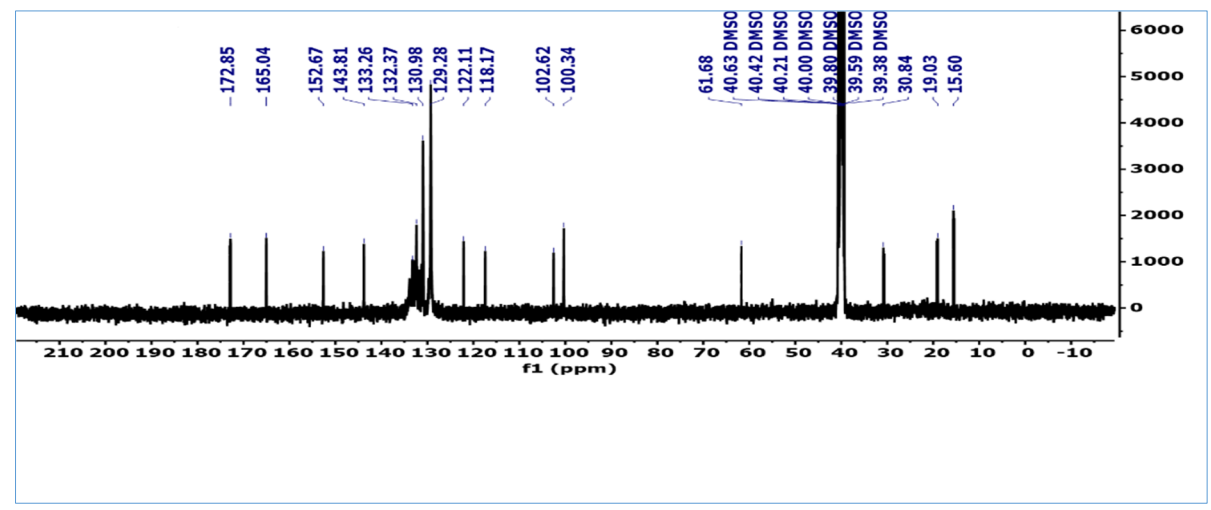


Fig. 12. ¹³C-NMR spectrum of the (H₁₅) compound

3.4. Nanomaterial Characterization

3.4.1. Characterization of the H₉ compound. X-ray diffraction spectra (XRD) and nanoscale properties for the compound [H₉] are shown in Fig. 13. These features include the number of layers (n = 10), the distance between the layers (d = 2.911), the grain size (D = 29), and the angle value (2θ = 30.7088).

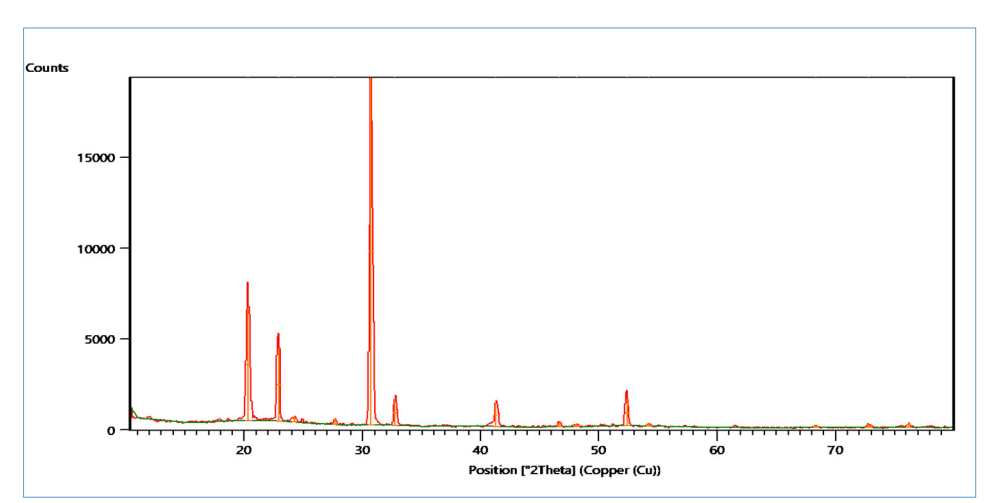


Fig. 13. XRD pattern of H₉-NPs

The morphology images of the [H9] compound in Figure 14 showed the presence of a 28.65 nm interlayer spacing in the sheet (a) and a low grain size in the sheet (b). This is attributed to the oxazepine ring linked to it, which led to an increase in the porosity of the sheets and a larger particle size, surface area, and thickening on the sheet. The roughness bias of the compound explains this due to the presence of active groups (Cl, Br, O) [27], as in Fig. 14.

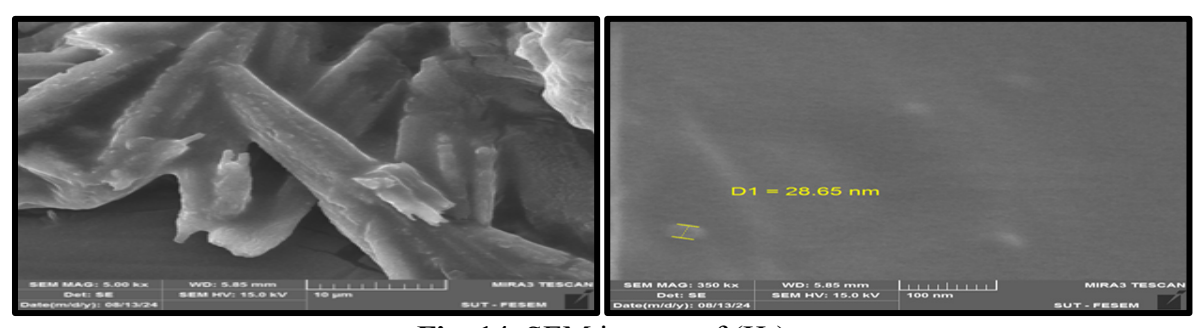


Fig. 14. SEM images of (H₉)

3.4.2. Characterization of the H_{13} . According to Fig. 15, the compound [H_{13}]'s XRD pattern revealed that its nanoscale properties include the number of layers (n = 7.8), the distance between the layers (d = 4.3383), the grain size (D = 17), and the angle value (20 = 20.4719).

The morphological images of the compound (H_{13}) in Figure 16 showed that the morphology of the compound was observed through scanning electron microscopy (SEM), with large particle size, increased plate porosity (b), division of the compound into high and transparent layers, and the presence of thickening on the plate (d), the presence of cracks on the surface, and deep cavities appeared, which is explained by the roughness bias of the compound, as the nano-size was 30.59 nm [28].

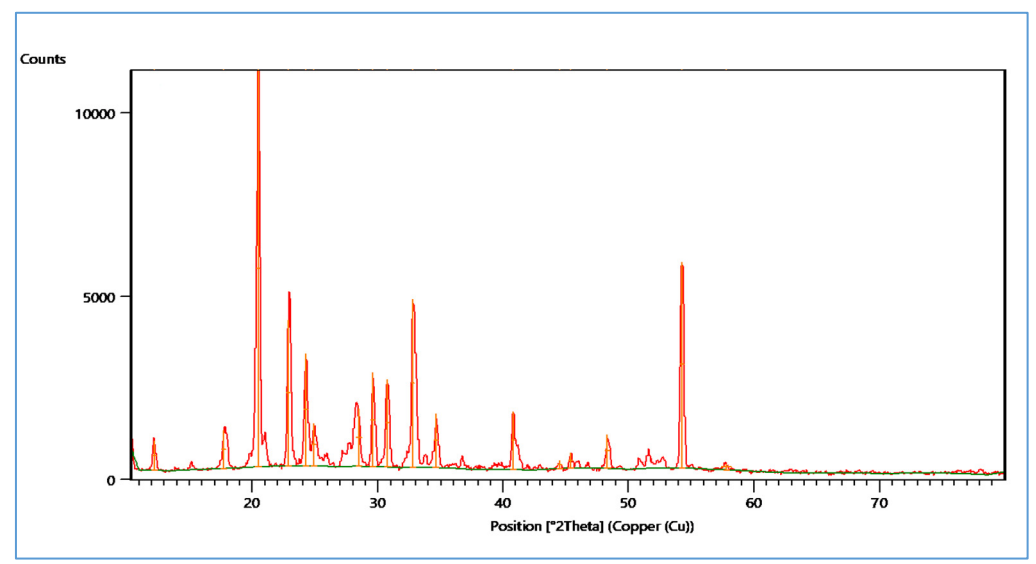


Fig. 15. XRD pattern of H₁₃-NPs

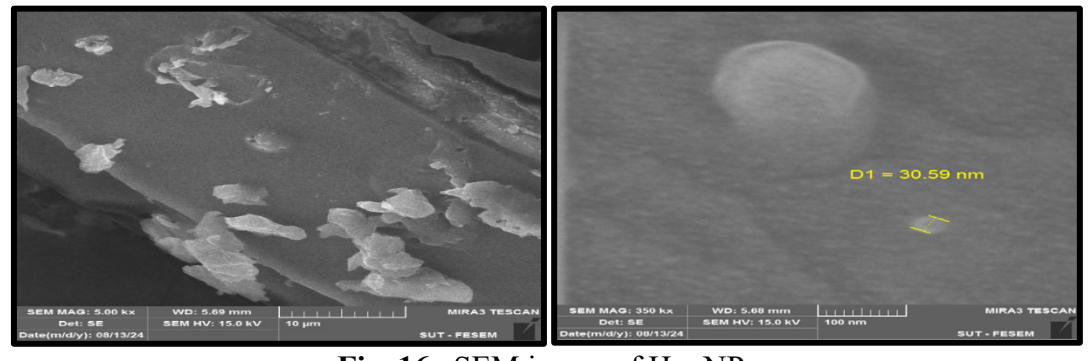


Fig. 16. SEM image of H₁₃-NPs

3.5. Laser Activity Measurement Results for Some Prepared Compounds. The analysis revealed that the chemical compounds' physical characteristics remained the same over the course of 15, 30, and 45 seconds since they were unaffected by the laser beams and retained their structural makeup. However, during the time period of 60 seconds, the physical properties changed, and there was a significant decrease in the melting points of all the studied compounds, along with a change in the flow (Rf) values in thin-layer chromatography (TLC) and a slight change in color. These changes likely led to the destruction of some bonds in the compounds, and it is possible that new compounds were formed as a result of the long and continuous exposure for a period of 60 seconds to high energy (laser beams), which led to the destruction of some bonds and the formation of new ones [29], as in Table 5.

Table 5. Results of measuring the laser effectiveness of some prepared compounds

Comp. 15 S	30 S	45 S	60 S
------------	------	------	------

	Color	M.P ⁰ C	Rf	Color	M.P ⁰ C	Rf	Color	M.P °C	Rf	Color	M.P °C	Rf
H_1	Light	124-	0.62	Light	124-	0.62	Light	124-	0.62	purple	111-	0.7
111	Purple	126	0.02	Purple	126	0.02	Purple	126	0.02	purpie	112	0.7
H ₅	Light	115-	0.65	Light	115-	0.65	Light	115-	0.65	araan	102-	0.55
П5	green	117	0.03	green	117	0.03	green	117	0.03	green	103	0.55
II.	0,000,000	245-	0.82	040400	245- 0.82	O#0# @0	245-	0.82	Red	231-	0.68	
H ₆	Orange	248		Orange	248	0.62	Orange	248	0.82	Keu	233	0.08
II.	Dark	247-	0.83	Dark	247-	0.83	Dark	247-	0.02	*******	235-	0.78
H_8	yellow	249	0.83	yellow	249	0.83	yellow	249	0.83 yellow		237	0.78
II.	White	217-	0.76	White	217-	0.76	White	217-	0.76	Vallary	203-	0.50
H ₁₂	White	219	0.76	White	hite 219		White	219	0.76	Yellow	205	0.59
11	Light	274-	0.75	Light	274-	0.75	Light	274-	0.75	0	253-	0.69
H ₁₃	Yellow	276	0.75	Yellow	276	0.75	Yellow	276	0.75	Orange	255	0.68

3.6. Evaluation of the Biological Activity of Prepared Compounds. Both Gram-positive and Gram-negative bacteria are targeted by heterocyclic chemicals, which have a variety of biological characteristics. In this investigation, the compounds' biological activity was assessed against two bacterial species: Staphylococcus aureus and Escherichia coli. These two species were chosen for their medical importance, as they cause various diseases. The zone of inhibition (cm) was calculated [30]. The results demonstrate that the prepared chemicals can inhibit the growth of both Grampositive and Gram-negative bacteria to varying degrees. Compounds H₅, H₈, and H₁₅ showed the most significant activity against S. aureus at all concentrations used, indicating their potential as high concentrations. Regarding E. coli, compounds H₅ and H₁₄ showed the highest inhibition at all concentrations. These compounds exceeded the effectiveness of the antibiotic used in the study, indicating their potential as future antibiotics. Other chemicals showed varying levels of activity [31]. Table 6 and Fig. s 17 and 18 show the compounds' ability to inhibit different types of bacteria.

Table 6. Biological effectiveness of prepared compounds and control treatments (inhibition in *cm*)

Comp. No.	Escherichia coil			Staphylococcus			
					S		
Conc. mg/ml	0.1	0.0	0.00	0.1	0.01	0.001	
		1	1				
H_1	2.5	2.0	15	1.7	2.0	1.0	
H ₄	3.0	3.3	20	1.5	1.3	1.0	
H ₅	3.5	1.0	35	4.0	3.7	3.5	
H ₇	1.5	1.3	7	1.5	1.5	1.5	
H ₈	2.1	2.3	9	3.5	3.9	3.8	
H_{10}	2.0	1.5	15	2.5	1.3	1.0	
H ₁₄	3.5	2.9	29	1.2	1.0	0.8	
H ₁₅	1.0	0.5	5	4.0	2.0	2.0	
Amoxicillin	2.0	2.0	10	2.4	1.6	1.0	

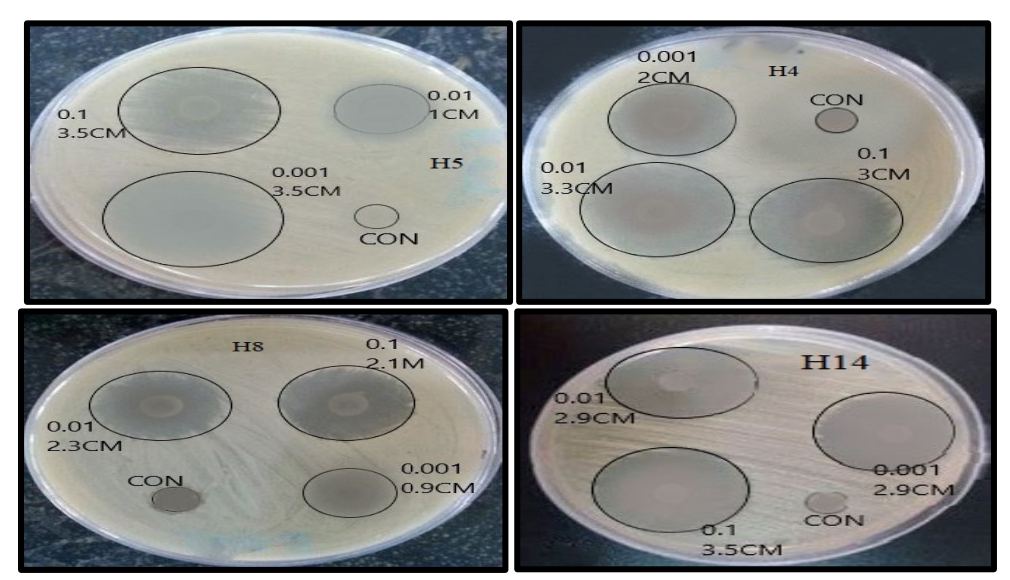


Fig. 17. Inhibitory effectiveness of compounds (H₁, H₄, H₈, and H₁₄) against *Escherichia coli*

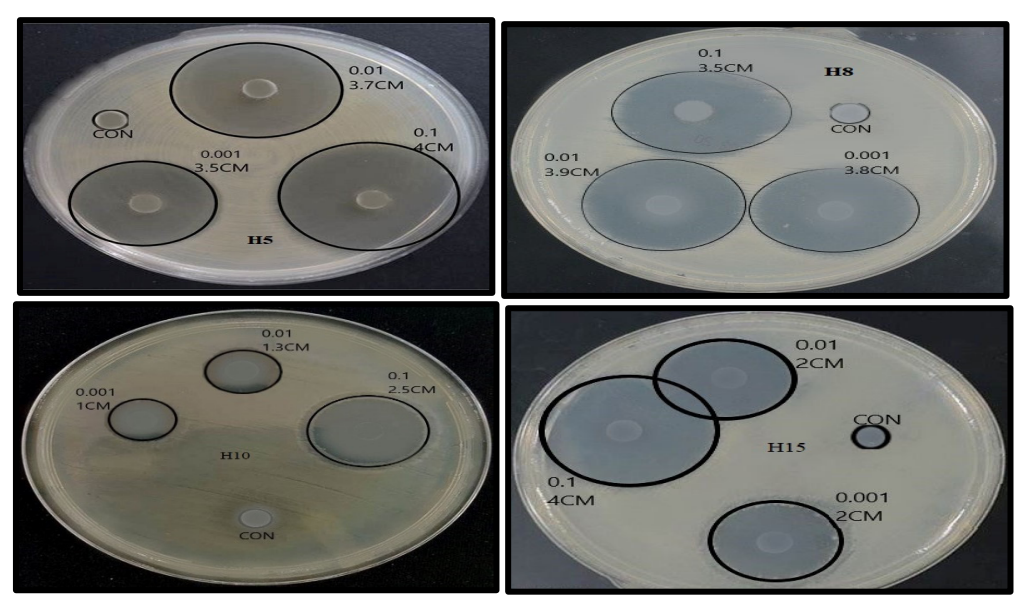


Fig. 18. Inhibitory effectiveness of compounds (H₅, H₈, H₁₀, and H₁₅) against Staph. Aureus

3.7. In Vitro Cytotoxicity Study on Breast Cancer (MCF-7) Cells. The ability of compounds [H₁₃, H₉] to inhibit the growth of MCF-7 cancer cells was tested using the in vitro cytotoxicity technique. The test was performed on the human mammary cancer cell line (MCF-7), where cells were exposed to five different concentrations of the prepared compounds (31.2, 62.5, 125, 250, and 500 µg/ml), in addition to negative and positive control samples. The absorbance (OD) was measured at each concentration, and the average absorbance was calculated for each concentration. The percentage of viable cells was also calculated based on the obtained values [32, 33]. The results showed a clear effect on the cytotoxicity of compound [H₉], with the cell viability rate being detailed below.

By examining the results of the cytotoxicity test and the effects on MCF-7 cancer cells at various concentrations, it can be observed that at high concentrations (500 and 250 μ g/ml), a significant decrease in cell viability was observed (54.64% and 84.79%, respectively), indicating that the prepared compound has a clear inhibitory effect on cancer cells, as in Fig. s 19 and 20.

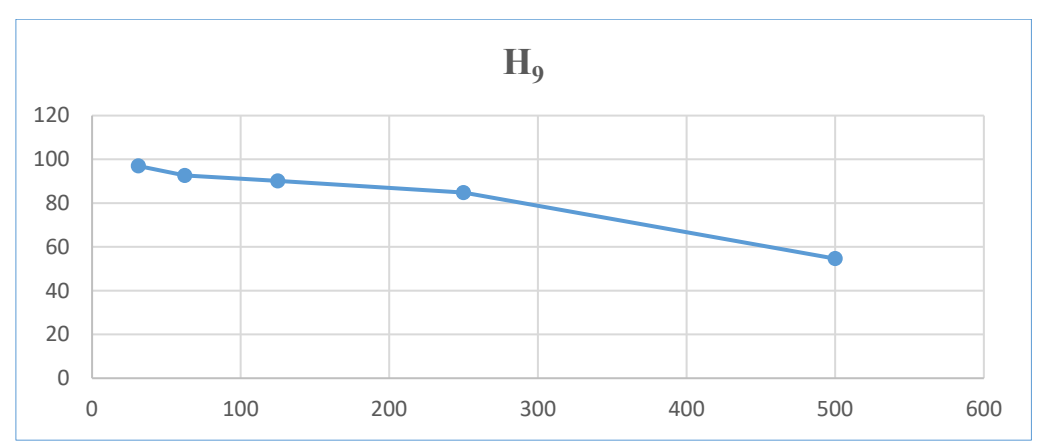


Fig. 19. The effect of compound (H₉) on MCF-7 cells using the MTT test

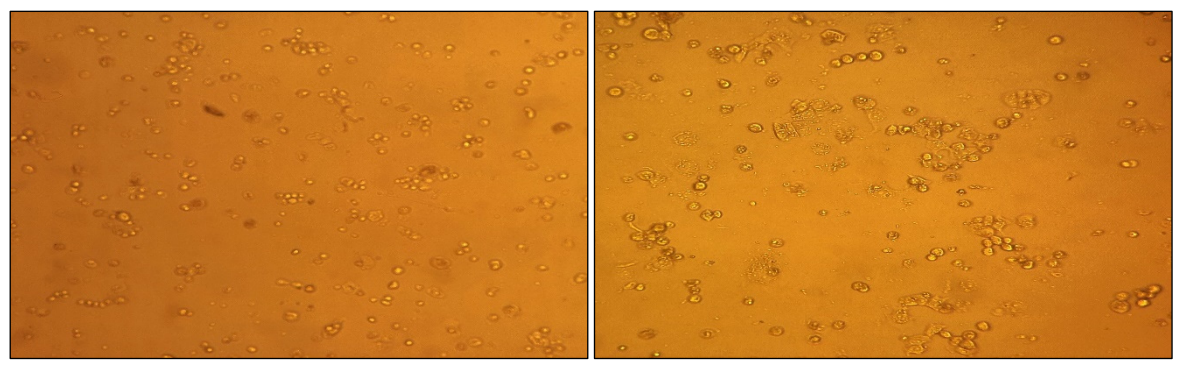


Fig. 20. The effectiveness of the compound (H₉) against breast cancer cells

When studying the effectiveness of compound [H13], the optical absorbance (OD) was measured at each concentration, and then the average absorbance for each concentration was calculated to determine the percentage of viable cells. The results showed a gradual decrease in cell viability with increasing concentration. These results indicate that the prepared compound has an inhibitory effect on cancer cells, becoming more pronounced with increasing concentration, especially at the 500 μ g/ml concentration, which showed a significant decrease in cell viability, making it close to the effect of the positive control (49.82%). In contrast, lower concentrations (31.2 and 62.5 μ g/ml) had a weak effect, indicating that the compound's efficacy is dose-dependent, as in Fig. s 21 and 22.

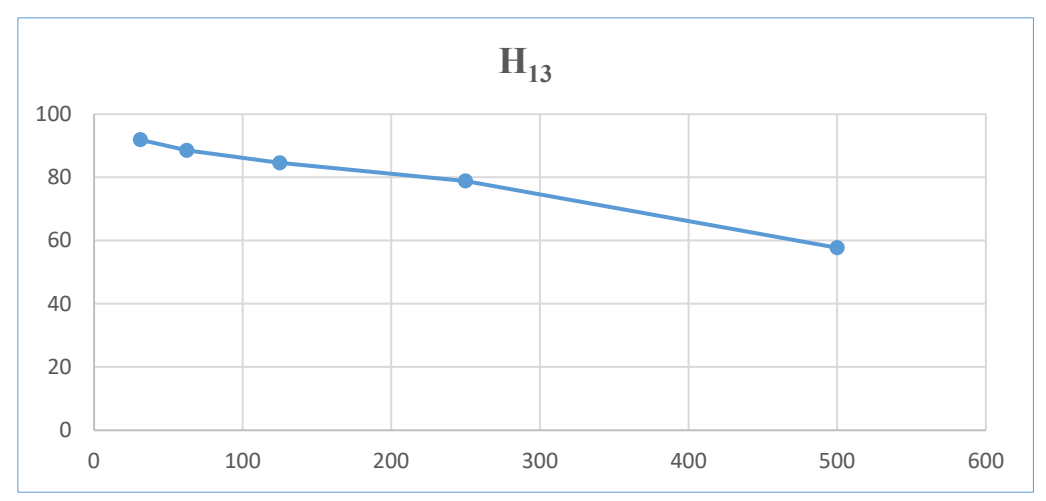


Fig. 21. The effect of compound (H₁₃) on MCF-7 cells using the MTT test

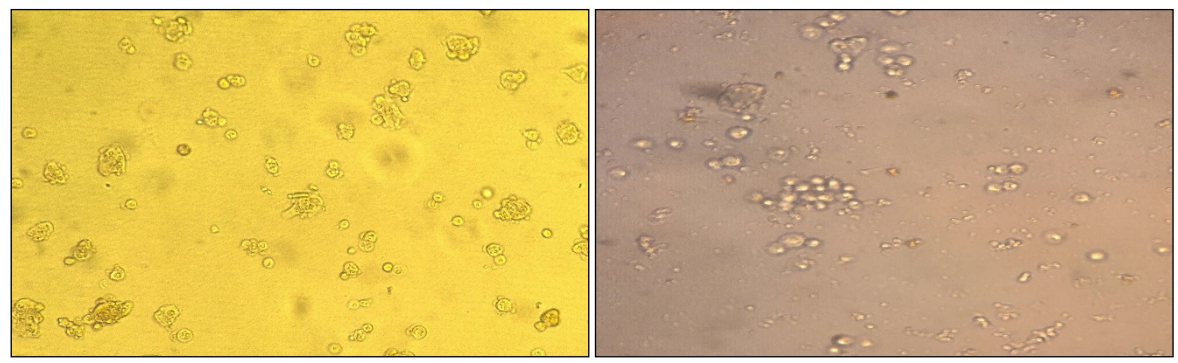


Fig. 22. The effectiveness of the compound (H₁₃) against breast cancer cells

3. Conclusions

Heterocyclic five-membered rings were created when hydrazide derivatives combine with substances that have appropriate functional groups. The majority of the produced compounds have antibacterial activity and may stop the development of germs, according to the findings of bioassays. Some of these substances even outperformed the antibiotics employed as controls in terms of biological activity. A few of the synthesized compounds demonstrated good activity against MCF-7 cancer cells. It was also shown that several of the synthesized compounds were stable when exposed to helium-neon laser light. Spectroscopic and physical studies validated the exact architectures of the produced nanocomposites.

References

- 1. Van Dooren A.A., Müller B.W. Purity determinations of drugs with differential scanning calorimetry (DSC)—a critical review. *International journal of pharmaceutics*, 1984, **Vol. (3)**, p. 217-233. DOI:10.1016/0378-5173(84)90170-4
- 2. Walsh C.T. Nature loves nitrogen heterocycles. *Tetrahedron Letters*, 2015, Vol. (23), p. 3075-3081. DOI:10.1016/j.tetlet.2014.11.046
- 3. Serrano-Wu M.H., Laurent D.R.S., Chen Y., Huang S., Lam K.R., Matson J.A., Mazzucco Ch.E., Stickle T.M., Tully Th.P., Wong H.S., Vyas D.M., Balasubramanian B.N. Sordarin oxazepine derivatives as potent antifungal agents. *Bioorganic & medicinal chemistry letters*, 2002, **Vol. (19)**, p. 2757-2760. DOI:10.1016/S0960-894X(02)00529-2
- 4. Mumit M.A., Pal T.K., Alam M.A., Islam M.A.A.A.A., Paul S., Sheikh M.C. DFT studies on vibrational and electronic spectra, HOMO–LUMO, MEP, HOMA, NBO and molecular docking analysis of benzyl-3-N-(2, 4, 5-trimethoxyphenylmethylene) hydrazinecarbodithioate. *Journal of molecular structure*, 2020, Vol. 1220, 128715. DOI:10.1016/j.molstruc.2020.128715
- 5. Baroudi B., Argoub K., Hadji D., Benkouider A.M., Toubal K., Yahiaoui A., Djafri A. Synthesis and DFT calculations of linear and nonlinear optical responses of novel 2-thioxo-3-N,(4-methylphenyl) thiazolidine-4 one. *Journal of Sulfur Chemistry*, 2020, Vol. (3), p. 310-325. DOI:10.1080/17415993.2020.1736073
- Jayathuna M.A., Ahmed S., Kim Y.G., Gajendiran M., Kim K., Rahiman A.K. Ferrocenylimine-based homoleptic metal (II) complexes: Theoretical, biocompatibility, in vitro anti-proliferative, and in silico molecular docking and pharmacokinetics studies. *Journal of Molecular Structure*, 2022, Vol. 1250, 131905. DOI: 10.1016/j.molstruc.2021.131905
- 7. Afridi H.H., Shoaib M., Al-Joufi F.A., Shah S.W.A., Hussain H., Ullah A., Zahoor M., Mughal E.U. Synthesis and investigation of the analgesic potential of enantiomerically pure schiff bases: a mechanistic approach. *Molecules*, 2022, **Vol.** (16), 5206. DOI:10.3390/molecules27165206
- 8. Ceramella J., Iacopetta D., Catalano A., Cirillo F., Lappano R., Sinicropi M.S. A review on the antimicrobial activity of Schiff bases: Data collection and recent studies. *Antibiotics*, 2022, **Vol.** (2), 191. <u>DOI: 10.3390/antibiotics11020191</u>

- Boukoucha N.H., Messasma Z., Aggoun D., Ouennoughi Y., Bensouici C., Fernández-García M., Lopez D., Guelfi M., Marchetti F., Bresciani G., Chorfi Z. Biological evaluation of a novel Schiff base ligand as an antioxidant agent: Synthesis, characterization and DFT computations of its Ni (II) and Cu (II) complexes. *Journal of Molecular Structure*, 2025, Vol. 1319, 139505. DOI:10.1016/j.molstruc.2024.139505
- 10. Sahu R., Shah K. Schiff Bases: A Captivating Scaffold with Potential Anticonvulsant Activity. *Mini Reviews in Medicinal Chemistry*, 2024, Vol. (18), p. 1632-1650. DOI:10.2174/0113895575302197240408121537
- 11. Bufarwa S.M., El-Sefait R.M., Thbayh D.K., Belaidi M., Al-Shemary R.K., Abdusamea R.M., El-Ajaily M.M., Fiser B., Bader H.A., Saleh A.A., Bufarwa M.M. Antituberculosis, antimicrobial, antioxidant, cytotoxicity and anti-inflammatory activity of Schiff base derived from 2, 3-diaminophenazine moiety and its metal (II) complexes: structural elucidation, computational aspects, and biological evaluation. *Reviews in Inorganic Chemistry*, 2024, Vol. (4), p. 105-124. DOI:10.1515/revic-2024-0007
- 12. Khaldoune K., Hasnaoui A., Fdil N., Oubella A., Lafhal K., Oubahmane M., Hdoufane I., El Ammari L., Saadi M., Berraho M., Ait Itto Y., El Firdoussi L., Ali M.A. Exploring anticancer activity, acute toxicity, and molecular docking of synthesized schiff bases and schiff base-palladium complex. *Inorganic Chemistry Communications*, 2023, Vol. 156, 111089. DOI:10.1016/j.inoche.2023.111089
- 13. Benzie I.F., Strain J.J. Ferric reducing/antioxidant power assay: direct measure of total antioxidant activity of biological fluids and modified version for simultaneous measurement of total antioxidant power and ascorbic acid concentration. In *Methods in enzymology*. 1999, **Vol. 299**, p. 15-27. DOI:10.1016/S0076-6879(99)99005-5
- 14. Hassan S.A., Aziz D.M., Abdullah M.N., Bhat A.R., Dongre R.S., Ahmed S., Rahiman A.K., Ben Hadda T., Berredjem M., Jamalis, J. Design and synthesis of oxazepine derivatives from sulfonamide Schiff bases as antimicrobial and antioxidant agents with low cytotoxicity and hemolytic prospective. *Journal of Molecular Structure*, 2023, Vol. 1292, 136121. DOI:10.1016/j.molstruc.2023.136121
- 15. Tsacheva I., Todorova Z., Momekova D., Momekov G., Koseva N. Pharmacological activities of Schiff bases and their derivatives with low and high molecular phosphonates. *Pharmaceuticals*, 2023, **Vol. (7)**, 938. DOI:10.3390/ph16070938
- 16. Khali, M.I. Synthesis and characterization of new oxazepine compounds derived from guanine. *Materials Today: Proceedings*, 2021, **Vol. 45**, p. 4960-4963. DOI:10.1016/j.matpr.2021.01.389
- 17. Niu L., Xing S., Li X., Chen H. Synthesis of the Fused Tetracyclic Thiazinan-4-one Derivatives and Their Anti-tumor Activity. *Chinese Journal of Organic Chemistry*, 2019, **Vol. 3**, 771. DOI:10.6023/cjoc201807043
- 18. Najm R.S., Shannak Q.A., Dalaf A.H. Synthesis and Decoration of Aromatic Derivatives Nano Platelets by the Electric Method. *Azerbaijan Pharmaceutical and Pharmacotherapy Journal*, 2023, Vol. (2), p. 92-97. DOI:10.61336/appj/22-2-22
- 19. Jumaa F.H., Yass E.A., Ibrahim B.K. Synthesis, Study of Their Liquid Crystal, Laser Properties of New Binary 1, 3-Oxazepine-4, 7-dione Derivatives and Evaluation of the Antibacterial Activity of Some of Them. *Journal of Global Scientific Research*, 2023, Vol. 8(9), p. 3201-3214. DOI:10.5281/zenodo.8312720
- 20. Salih B.D., Dalaf A.H., Alheety M.A., Rashed W.M., Abdullah I.Q. Biological activity and laser efficacy of new Co (II), Ni (II), Cu (II), Mn (II) and Zn (II) complexes with phthalic anhydride. *Materials Today: Proceedings*, 2021, **Vol. 43**, p. 869-874. DOI: 10.1016/j.matpr.2020.07.083
- 21. Aftan M.M., Toma M.A., Dalaf A.H., Abdullah E.Q., Salih H.K. Synthesis and characterization of new azo dyes based on thiazole and assess the biological and laser efficacy for them and study their dyeing application. *Egyptian Journal of Chemistry*, 2021, **Vol. (6)**, p. 2903-2911. DOI:10.21608/ejchem.2021.55296.3163

- 22. Alasadi Y.K., Jumaa F.H., Dalaf A.H., Shawkat S.M., Mukhlif M.G. Synthesis, Characterization, and Molecular Docking of New Tetrazole Derivatives as Promising Anticancer Agents. *Journal of Pharmaceutical Negative Results*, 2022, **Vol. (3)**, p. 513-522. DOI:10.47750/pnr.2022.13.03.079
- 23. Jóźwiak M., Filipowska A., Fiorino F., Struga M. Anticancer activities of fatty acids and their heterocyclic derivatives. *European journal of pharmacology*, 2020, **Vol. 871**, 172937. DOI:10.1016/j.ejphar.2020.172937
- 24. Salihović M., Pazalja M., Halilović S.Š., Veljović E., Mahmutović-Dizdarević I., Roca S., Novaković I., Trifunović S. Synthesis, characterization, antimicrobial activity and DFT study of some novel Schiff bases. *Journal of molecular structure*, 2021, **Vol.** 1241, 130670. DOI:10.1016/j.molstruc.2021.130670
- 25. Vessally E., Hosseinian A., Edjlali L., Bekhradnia A., Esrafili M.D. New route to 1, 4-oxazepane and 1, 4-diazepane derivatives: synthesis from N-propargylamines. *RSC Advances*, 2016, **Vol. 102(6)**, p. 99781-99793. DOI:10.1039/C6RA20718A
- 26. das Neves A.M., Campos J.C., Gouvêa D.P., Berwaldt G.A., Goulart T.B., Avila C.T., Machado P., Zimmer G.C., #Cunico W. Synthesis of Novel Thiazolidin-4-ones and Thiazinan-4-ones Analogous to Rosiglitazone. *Journal of Heterocyclic Chemistry*, 2019, Vol. (1), p. 251-259. DOI:10.1002/jhet.3402
- 27. Najm R.S., Al-Somaidaie G.H. Carbonation and preparation of reduced graphene oxide sheets from cellulose. In 39th PATTAYA International Conference on "Advances in Chemical, Agriculture, Biology & Environment" (PCABE-22) Pattaya (Thailand) Aug. 2022, Vol. 25, p. 25-26. DOI:10.17758/DIRPUB12.DIR0822212
- 28. Kumar P.S., Padmalaya G., Elavarasan N., Sreeja B.S. A selective analysis of sulfamethoxazole—Trimethoprim in tablet formulations using graphene oxide-zinc oxide quantum dots based nanocomposite modified glassy carbon electrode. *Chemosphere*, 2023, **Vol. 332**, 138814. DOI:10.1016/j.chemosphere.2023.138814
- 29. Saleh R.H., Rashid W.M., Dalaf A.H., Al-Badrany K.A., Mohammed O.A. Synthesis of some new thiazolidinone compounds derived from schiff bases compounds and evaluation of their laser and biological efficacy. *Ann Trop & Public Health*, 2020, **Vol.** (7), p. 1012-1031. DOI:10.36295/ASRO.2020.23728
- 30. Abdullah S.H., Salih M.M., Al-Badrany A. Synthesis, Characterization and Antibacterial Evaluation of Novel Thiazolidine Derivatives. *Journal of Angiotherapy*, 2024, **Vol. (3)**, p. 1-9. DOI:10.25163/angiotherapy.839501
- 31. Muhammad F.M., Khairallah B.A., Albadrany K.A. Synthesis, characterization and antibacterial evaluation of novel 1, 3-oxazepine derivatives using a cycloaddition approach. *Journal of Angiotherapy*, 2024, Vol. (3), p. 1-5. DOI:10.25163/angiotherapy.839506
- 32. Kumar N., Goel N. Heterocyclic compounds: importance in anticancer drug discovery. *Anti-Cancer Agents in Medicinal Chemistry-Anti-Cancer Agents*, 2022, **Vol. (19)**, p. 3196-3207. DOI: 10.2174/1871520622666220404082648
- 33. Hosseinzadeh Z., Ramazani A., Razzaghi-Asl N. Anti-cancer nitrogen-containing heterocyclic compounds. *Current Organic Chemistry*, 2018, Vol. 22(23), p. 2256-2279. DOI:10.2174/1871520622666220404082648